As seen in (11), the irregular contribution appears since there is a discontinuity in the arc length. In other words $\mathbf{H}_{1D}(\mathbf{r},t)$ appears whether $d=0$ or $d\neq 0$ since arc length has a discontinuity. But if $d\neq 0$, there is a retardation in time, taking place in the Dirac delta function. This retardation appears in the argument of the temporal basis as $T_i(t-d/c)$.

Another case appears when the testing and basis patches are different but have a common edge, i.e., neighbor-testing. The discontinuity in the arc length is seen only if the observation point is on this common edge. When the observation point is on the edge of the source patch, as mentioned above, $d=0$ and one of the area coordinates is zero. Unfortunately normal vectors of the test and basis patches are not the same in this case. Hence, $\hat{\mathbf{n}}\cdot(\boldsymbol{\rho}-\boldsymbol{\rho}_n)\neq 0$ and $\hat{\mathbf{n}}\cdot\hat{\mathbf{n}}'\neq 1$. As in the self-term evaluation, there is a contribution from $\mathbf{H}_{1D}(\mathbf{r},t)$, because of the discontinuity in arc length. Also it can be shown that $\mathbf{H}_{1R}(\mathbf{r},t)$ in (10), yields zero because $d=0$. However, $\mathbf{H}_2(\mathbf{r},t)$ is not always zero because $\hat{\mathbf{n}}\cdot\hat{\mathbf{n}}'\neq 1$. In this case, a contribution from $\mathbf{H}_2(\mathbf{r},t)$ must be evaluated. The frequency domain counterpart of this case is investigated in [5].

III. Conclusions

In this work, singularity of the time domain magnetic field is investigated for the MOT solution of the MFIE and a general form for the singular contribution is derived with no approximations or limiting procedures. It is shown that the singular contribution depends on the location of the observer on the support of the basis function. Also while the observation point is within the basis patch, it is shown that the well-known one half factor is obtained.

References

[1] R. E. Collin, *Field Theory of Guided Waves*, 2nd ed. New York: IEEE Press, 1990.

[2] M. I. Sancer, "MFIE limiting process and curvilinear computations," in *Proc. 1998 IEEE AP-S Int. Symp.*, Atlanta, GA, vol. 2, pp. 886–887.

[3] R. E. Hodges and Y. Rahmat-Samii, "The evaluation of MFIE integrals with the use of vector triangle basis functions," *Microw. Opt. Tech. Lett.*, vol. 14, no. 1, pp. 9–14, Jan. 1997.

[4] L. Gürel and Ö. Ergül, "Singularity of the magnetic-field integral equation and its extraction," *IEEE Antenna Wireless Propag. Lett.*, vol. 4, pp. 229–231, 2005.

[5] Ö. Ergül and L. Gürel, "Solid-angle factor in the magnetic field integral equation," *Microw. Opt. Tech. Lett.*, vol. 45, no. 5, pp. 452–456, Jun. 2005.

[6] J. M. Ruis, E. Udeba, and J. Parron, "On the testing of the magnetic field integral equation with RWG basis functions in method of moments," *IEEE Trans. Antennas Propag.*, vol. 49, no. 11, pp. 1550–1553, Nov. 2001.

[7] S. M. Rao, D. R. Wilton, and A. W. Glisson, "Electromagnetic scattering by surfaces of arbitrary shape," *IEEE Trans. Antennas Propag.*, vol. 30, no. 3, pp. 408–418, May 1982.

[8] H. A. Ülkü and A. A. Ergin, "Analytical evaluation of transient magnetic fields due to RWG current bases," *IEEE Trans. Antennas Propag.*, vol. 55, no. 12, pp. 3565–3575, Dec. 2007.

[9] H. A. Ülkü and A. A. Ergin, "Application of analytical expressions of transient potentials to the MOT solution of integral equations," presented at the 2008 IEEE AP-S Int. Symp. and URSI Radio Science Meeting, San Diego, CA.

Fast Computation of Sommerfeld Integral Tails via Direct Integration Based on Double Exponential-Type Quadrature Formulas

Ružica Golubović Nićiforović, Athanasios G. Polimeridis, and Juan R. Mosig

***Abstract*—A direct integration algorithm, based on double exponential-type quadrature rules, is presented for the efficient computation of the Sommerfeld integral tails, arising in the evaluation of multilayered Green's functions. The proposed scheme maintains the error controllable nature of the so-called partition-extrapolation methods, often used to tackle this problem, whereas it requires substantially reduced computational time. Moreover, the proposed method is very easy to implement, since the associated weights and abscissas can be precomputed. The overall behavior of the proposed method both in terms of accuracy and efficiency is demonstrated through a series of representative numerical experiments, where compared with one of the most proven methods available in the literature.**

***Index Terms*—Mixed potential integral equations, multilayered Green's functions, Sommerfeld integrals.**

I. Introduction

Planar technologies, in which thin metallizations are embedded within stratified dielectric media, are one of the most popular and successful approaches to build circuits and antennas in microwaves and millimeter waves with a good performance-to-price ratio. One of the most proven mathematical models to analyze these structures is based on the integral equation formulations, combined with a Galerkin method of moments (MoM) approach for the numerical solution [1]–[3]. Among several possible variants, the mixed potential integral equation (MPIE) formulation is generally considered to be more efficient for numerical modeling of arbitrary shaped printed circuits, because it requires only the potential forms of Green's functions, which are less singular than their derivatives, usually involved in electric and magnetic field integral equations.

The solution of MPIE via MoM calls for the fast and accurate computation of the associated Green's functions in spatial domain, which are Fourier-Bessel integral transforms, commonly known as Sommerfeld integrals (SIs), i.e., semi-infinite range integrals with Bessel function kernels. Due to the highly oscillating and slowly decaying nature of the integrands, the numerical evaluation of the SIs is very time consuming. Generally, several methods have been proposed in order to tackle this problem, which can be roughly categorized into two main families: First, we could mention the closed-form Green's functions methods (see [4]–[8] among others), where no numerical integration is needed. Instead, the integrand (spectral-domain Green's function) is approximated via a finite sum of special functions, such that their SIs admit analytical evaluation. Although Green's functions need to be evaluated only once for all transverse distances via the aforementioned methods,

Manuscript received January 21, 2010; revised June 09, 2010; accepted July 01, 2010. Date of publication December 03, 2010; date of current version February 02, 2011. This work was supported in part by the European COST Action IC0603 "ASSIST".

The authors are with the Laboratory of Electromagnetics and Acoustics (LEMA), Ecole Polytechnique Fédérale de Lausanne (EPFL), CH-1015 Lausanne, Switzerland (e-mail: ruzica.golubovic@epfl.ch; athanasios.polymeridis@epfl.ch; juan.mosig@epfl.ch).

Color versions of one or more of the figures in this communication are available online at http://ieeexplore.ieee.org.

Digital Object Identifier 10.1109/TAP.2010.2096187

their complete lack of a priori error control still remains a critical challenge for the future. As an alternative, the second family consists of all methods that are based on the numerical integration of the SIs. More specifically, it is the tail of SIs that requires a special treatment, like the so-called integration-then-summation procedure combined with one of the numerous extrapolation techniques for the convergence acceleration, among which the weighted averages (WA) method is proven to be one of the most efficient [9], [10]. Alternatively, one could also choose the direct integration of the SIs as suggested in [11]–[14]. Finally, a somewhat hybrid approach was introduced in [15], where the integrand of the SI tail is fitted by a sum of finite complex exponentials, similar to the philosophy of closed-form Green's functions methods, leaving a remainder to be numerically evaluated.

In this communication, we present a novel technique for the fast and accurate computation of SI tails via direct integration, based on Double Exponential (DE)-type quadrature formulas [16]. The key feature of the proposed scheme is its error controllable behavior, while comprising a superior performance, in terms of efficiency, against the traditional integration-then-summation procedure, which is considered as the most robust method for treating the SI tails. The DE quadrature formula was introduced in the mid-seventies [17] and, since then, it has gradually come to be used widely in various fields of science and engineering. The originally proposed formula was intended for the evaluation of the integrals with endpoint singularities and lacked efficiency when evaluating an integral of a slowly decaying oscillatory function over semi-infinite intervals. In order to overcome this weakness, the idea of using the Bessel function zeros as integration points of quadrature formulas was employed in [18], in the case of exponential-type entire functions, with a further elaboration in [19], [20]. The final outcome of this research was a very efficient tool for the evaluation of integral tails with Bessel function kernels [16]. This general algorithm is adapted in this communication to tackle a persistent problem in computational electromagnetics: the Sommerfeld integral tail.

In Section I, a brief introduction about the SI tails and the extrapolation methods often used as convergence accelerators within integration-then-summation procedure, is presented. The DE quadrature formula tailored for the Sommerfeld-type integrals is developed in detail in Section II. Finally, in Section III, a comparison of the proposed method with the best candidate of the extrapolation methods is presented in terms of accuracy and efficiency. The results obtained therein fully justify the use of such sophisticated quadrature rules for treating the SI tails.

II. Sommerfeld Integral Tails

With reference to the generic layered media of Fig. 1, the Sommerfeld-type integrals can be written as follows [10]:

$$S_n\left\{\tilde{G}(k_\rho;z|z')\right\}=\frac{1}{2\pi}\int_0^\infty \tilde{G}(k_\rho;z|z')\mathrm{J}_n(k_\rho\rho)k_\rho dk_\rho \qquad (1)$$

where $\tilde{G}$ is the spectral domain Green's function of the layered media, J_n is the Bessel function of the first kind of order n, ρ is the horizontal distance between the field and source points, and z, z' are the vertical coordinates of those points, respectively. Since SIs possess singularities on and/or near the real axis, it is well known [21] that the semi-infinite integral path must be deformed into the imaginary positive part of the complex spectral (k_ρ) plane to avoid them (Fig. 2). Therefore, we split our generic Sommerfeld integral as

$$S_n=\frac{1}{2\pi}(I_n+T_n). \qquad (2)$$

The integration path for I_n joins the origin to a point ξ_0 on the real axis, conveniently distant from the singularities. Typically, part of it or its entirety goes into the complex plane (Fig. 2). Techniques for adaptively selecting the integration path and for numerically evaluating I_n have been discussed elsewhere [21].

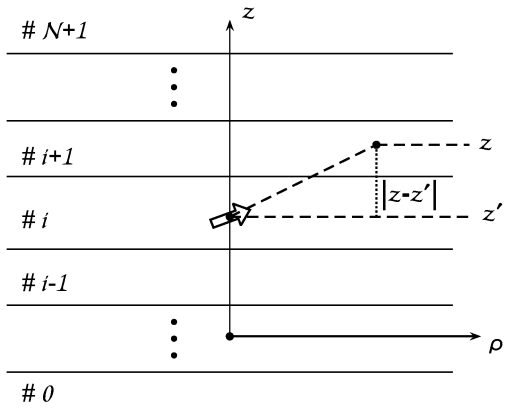

Fig. 1. Generic stratified media showing a point source (level z') and a field observation point (level z) separated by a radial distance ρ. The medium can be terminated or not by PEC, PMC and impedance planes.

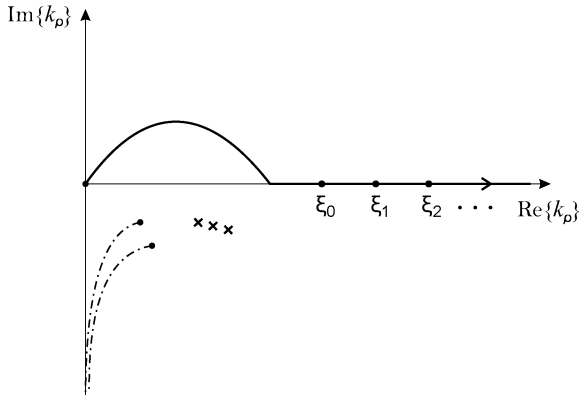

Fig. 2. Deformed integration path for the computation of Sommerfeld integrals.

The remaining integral

$$T_n=\int_{\xi_0}^\infty \tilde{G}(k_\rho;z|z')\mathrm{J}_n(k_\rho\rho)k_\rho dk_\rho \qquad (3)$$

is the Sommerfeld tail where the integration path is a semi-infinite integral $[\xi_0,\infty]$ on the real axis. This tail is traditionally evaluated as a sum of partial integrals over the finite subintervals (integration-then-summation procedure) [10]

$$T_n=\sum_{i=0}^\infty u_{n_i}=\sum_{i=0}^\infty \int_{\xi_i}^{\xi_{i+1}} \tilde{G}(k_\rho;z|z')\mathrm{J}_n(k_\rho\rho)k_\rho dk_\rho. \qquad (4)$$

Possible choices for the breakpoints ξ_i include the asymptotic half-periods, exact zero crossings and extrema of Bessel functions [10]. The sum in (4) converges extremely slowly, thus, calling for suitable acceleration techniques, often referred as extrapolation methods. Among the numerous techniques that are traditionally used as convergence accelerators for the evaluation of SI tails, WA method with the asymptotic calculation of remainder estimates is shown to be one of the most versatile and efficient. WA method was originally developed by Mosig [22]–[24], with a further elaboration by Michalski [10], and is also referred in the literature as the Mosig-Michalski transformation [25].

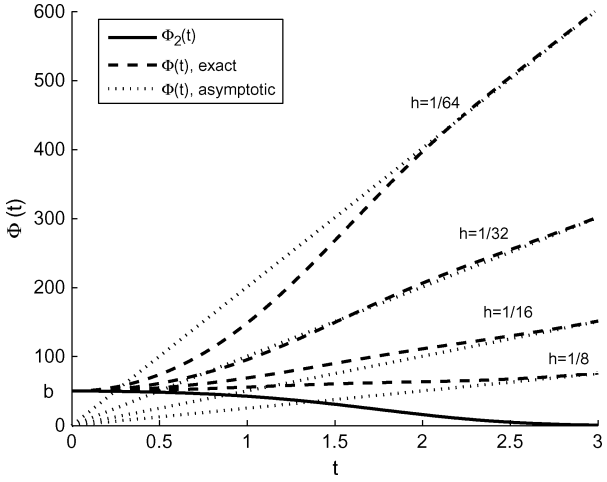

Fig. 3. Behavior of the DE transformation for different values of step size parameter h.

Next, we introduce a new strategy for the evaluation of the Sommerfeld tails and we will compare it with a WA approach using the Mosig-Michalski algorithm.

III. Double Exponential-Type Quadrature Formulas

The DE formula is the generic name of a family of optimal quadrature formulas based on the DE transformation and it was originally introduced by Takahasi and Mori in 1974 [17]. The first DE quadrature rule was tailored for integrals with integrable singularities at the end of the integration interval. Recently, Ooura and Mori proposed a novel DE-type quadrature formula for tackling Fourier-type integrals, i.e. semi-infinite range integrals with sinusoidal function kernels [26]. Following the same philosophy, Ogata and Sugihara introduced a DE-type quadrature formula with Bessel function zeros as nodes, for the Hankel transform integrals [16].

Here we use the aforementioned original study by Ogata and Sugihara [16] in order to introduce the following transformation (specifically tailored for the SI tails of our interest)

$$k_\rho \cdot \rho = \Phi(t) \tag{5}$$

with

$$\begin{aligned}\Phi(t) &= \frac{\pi}{h} t \cdot \tanh\left(\frac{\pi}{2}\sinh(t)\right) + b \cdot \operatorname{sech}\left(\frac{\pi}{2}\sinh(t)\right) \\ &= \Phi_1(t) + \Phi_2(t)\end{aligned} \tag{6}$$

where $b = \xi_0 \cdot \rho$ and h is the so-called step size that has to be chosen carefully since it directly influences the algorithm performance.

In Fig. 3 the transformation $\Phi(t)$ is shown for different values of the step size h. The role of the second part of the transformation (6), $\Phi_2(t)$, is actually to map the starting point of the integration interval from $k_\rho = \xi_0$ into $t = 0$, and its influence vanishes quickly as $t \longrightarrow \infty$. The first part of the transformation, $\Phi_1(t)$, has the dominant effect for the higher values of t, approaching rapidly the transformation's asymptotic behavior, $\Phi(t) \sim (\pi/h)|t|$, that will be shown later to be the key attribute of the method.

Applying the aforementioned transformation to the SI tail (3), we obtain

$$T_n = \int_0^\infty \mathcal{F}_n\left(\Phi(t)\right) \cdot \left(\frac{d\Phi(t)}{dt}\right) dt \tag{7}$$

where

$$\mathcal{F}_n(t) = \frac{1}{\rho^2} t \cdot \tilde{G}\left(\frac{1}{\rho}t; z|z'\right) \cdot \mathrm{J}_n(t). \tag{8}$$

Since the integrand in (7) is an odd function with respect to t, the integral can be written as

$$T_n = \frac{1}{2}\int_{-\infty}^{\infty} \operatorname{sgn}(t) \cdot \mathcal{F}_n\left(\Phi(t)\right) \cdot \left(\frac{d\Phi(t)}{dt}\right) dt \tag{9}$$

and approximated with the help of an appropriate quadrature formula based on the zeros of Bessel functions, according to [16],

$$\begin{aligned}T_n \approx\ & h\sum_{k=1}^{\infty} w_{nk}\mathcal{F}_n\left(\Phi\left(h\frac{\xi_{nk}}{\pi}\right)\right)\Phi'\left(h\frac{\xi_{nk}}{\pi}\right) \\ & + \frac{h}{\pi}\sum_{\lambda=0}^{n-1} c_\lambda^{(n)} h^{2\lambda+1} \left.\frac{\partial^{2\lambda+1}\left\{\mathcal{F}_n\left(\Phi(t)\right)\Phi'(t)\right\}}{\partial t^{2\lambda+1}}\right|_{t=0}\end{aligned} \tag{10}$$

where ξ_{nk} is the k-th zero of the Bessel function J_n. Also

$$c_\lambda^{(n)} = \frac{\pi^{-2\lambda+1}}{(2\lambda+1)!}\sum_{m=0}^{n-\lambda-1}\frac{(n-m-1)!}{m!}2^{n-2m}b_{n-\lambda-m-1}^{(n)} \tag{11}$$

and $b_m^{(n)}$, $m = 0, 1, 2, \ldots$, are the coefficients of the Laurent series expansion of $1/\mathrm{J}_n$ around the point $x = 0$:

$$\frac{1}{\mathrm{J}_n(x)} = \sum_{m=0}^{\infty} b_m^{(n)} x^{2m-n}. \tag{12}$$

Moreover, the weights w_{nk} are given as follows:

$$w_{nk} = \frac{\mathrm{Y}_n(\xi_{nk})}{\mathrm{J}_{n+1}(\xi_{nk})} = \frac{2}{\pi\xi_{nk}\mathrm{J}_{n+1}^2(\xi_{nk})}. \tag{13}$$

Finally, after some algebraic manipulations, we derive the DE-type quadrature formulas for the SI tails (3). In particular, for the two most used indexes $n = 0$, 1 of the Bessel functions, we get

$$T_0 \approx h\sum_{k=1}^{N} w_{0k}\mathcal{F}_0\left(\Phi\left(h\frac{\xi_{0k}}{\pi}\right)\right)\Phi'\left(h\frac{\xi_{0k}}{\pi}\right) \tag{14}$$

and

$$\begin{aligned}T_1 \approx\ & h\sum_{k=1}^{N} w_{1k}\mathcal{F}_1\left(\Phi\left(h\frac{\xi_{1k}}{\pi}\right)\right)\Phi'\left(h\frac{\xi_{1k}}{\pi}\right) \\ & + \left(2h - \frac{1}{2}bh^2\right)\mathcal{F}_1(b).\end{aligned} \tag{15}$$

Actually, the key feature of the aforementioned transformation is that since $\Phi(t) \sim (\pi/h)|t|$ double exponentially as $t \to \pm\infty$ (shown in Fig. 3), the quadrature nodes of the final formulas approach double exponentially to the zeros of the associated Bessel functions, i.e., $\Phi(h(\xi_{nk}/\pi)) \sim \xi_{nk}$ as $k \to \infty$. More specifically, for large values of k we have

$$\mathrm{J}_n\left(\Phi\left(h\cdot\frac{\xi_{nk}}{\pi}\right)\right) \simeq \mathrm{J}_n\left(\frac{\pi}{h}\cdot h\cdot\frac{\xi_{nk}}{\pi}\right) = 0 \tag{16}$$

allowing us to truncate the infinite sum (10) at moderate N, as shown in (14), (15), without loss of accuracy.

IV. Numerical Results

In this section, we perform several numerical experiments in order to demonstrate the accuracy and efficiency of the formulas presented in (14) and (15). For the sake of comparison, we choose one of the

most proven methods for the evaluation of the SI tails: the integration-then-summation procedure combined with the WA method and utilizing equidistant break points separated by the asymptotic half-period of the associated Bessel functions [10]. While, thanks to the Sommerfeld identity, analytical solutions exist for a family of Sommerfeld integrals (for instance the free-space case), nothing comparable can be said for Sommerfeld tails, especially if their starting point $\xi_0 = b$ is taken at an arbitrary point of the real axis. This amounts to say that for very simple layered problems we can rearrange formula (2) as

$$T_n = S_n - I_n = \text{analytical value} - I_n. \tag{17}$$

Therefore, if we try in these cases to assess the absolute error or precision of an algorithm for evaluating the tail T_n, we need to be sure that we are numerically evaluating the finite integral I_n with the best precision, close to machine precision if possible. Two basic tails can be obtained by applying the scheme in (17) to the Sommerfeld integrals:

$$\int_b^\infty \frac{e^{-jk_z|z|}}{jk_z} \mathrm{J}_0(k_\rho\rho)k_\rho dk_\rho = \frac{e^{-jkr}}{r} - \int_0^b \frac{e^{-jk_z|z|}}{jk_z} \mathrm{J}_0(k_\rho\rho)k_\rho dk_\rho \tag{18}$$

and to the ρ-derivative of the above

$$\int_b^\infty \frac{e^{-jk_z|z|}}{jk_z} \mathrm{J}_1(k_\rho\rho)k_\rho^2 dk_\rho = (1+jkr)\frac{\rho e^{-jkr}}{r^3} - \int_0^b \frac{e^{-jk_z|z|}}{jk_z} \mathrm{J}_1(k_\rho\rho)k_\rho^2 dk_\rho \tag{19}$$

where $k_z = \sqrt{k^2 - k_\rho^2}$. The integrals I_n in the right-hand sides of (18), (19) are computed to machine precision by an adaptive quadrature based on the Patterson's formulas [27]. Then the tails T_n (integrals in the left-hand sides of (18), (19)) are evaluated with the WA algorithm and with our DE technique. In the WA algorithm, the partial integrals u_{n_i} in (4) must be computed using a Gauss-Legendre quadrature of order 16, as suggested in [21], because in the case of negligibly small integrands, numerical experiments have shown that adaptive Patterson quadrature rule can fail trying to integrate what is essentially numerical noise.

The key parameter in the DE quadrature is the step size h in (14), (15). It directly influences the performance of the formulas and, therefore, it has to be chosen carefully. We have found experimentally that the value $h = 1/32$ stands as the best trade-off between accuracy and computational cost for the SI tails. We also set, following again the suggestions in [10], a maximum of 160 integration points (ten integration intervals for WA method) for both algorithms, if the predefined accuracy (10 eps) is not reached.

In Figs. 4(a) and 4(b), the number of significant digits of the relative error in the evaluation of the Sommerfeld identity tail (18) and its ρ-derivative (19) versus $k_0\rho$ for the most challenging case, i.e., $z = 0$, is presented. While both methods provide very accurate results, the DE-type algorithm needs in average up to 25% less integration points than WA method. In this point, we need to mention that a comparison in terms of integration points reflects also the relative computational time, since the overhead of the WA method has the same effect as the computation of more complicated kernels in the DE-type method.

Next, we proceed to a more elaborate numerical experiment including a wide range of distances from the source $(-3 \le \log_{10}(k_0\rho), \log_{10}(k_0 z) \le 1)$. To be more specific, the relative number of integration points $N_{\mathrm{DE}}/N_{\mathrm{WA}}$ (%) is presented in Figs. 5(a) and 5(b) for the tails of (18) and (19), respectively. Again,

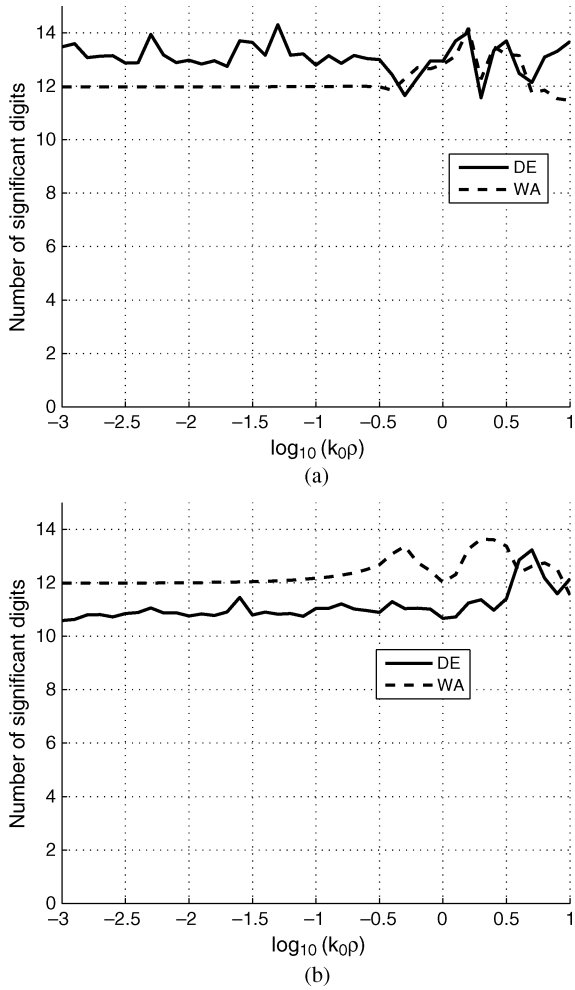

Fig. 4. Performance of DE formulas (14), (15) and WA method for $z = 0$. (a) Sommerfeld identity tail (18). (b) Derivative of the Sommerfeld identity tail (19).

upon discarding the lower part of the Figures, where basically the contribution of the tail is zero, it is clear that the proposed integration scheme is much more efficient than the WA method in a plethora of observation points.

In the end, we will demonstrate the worthiness of the proposed scheme in two *real life* applications, i.e., a three-layer geometry ($f = 8$ GHz):

- layer-0: PEC;
- layer-1: $\epsilon_{r1} = 4$, $d_1 = 1\lambda$;
- layer-2: free-space.

and a four-layer geometry ($f = 1, 30$ GHz):

- layer-0: PEC;
- layer-1: $\epsilon_{r1} = 4$, $d_1 = 0.1$ cm;
- layer-2: $\epsilon_{r2} = 12.6$, $d_2 = 0.1$ cm;
- layer-3: free-space.

In both cases, the source (HED) is placed at the interface between the dielectric stack and the free-space. Also, we consider only the most challenging case when the observation plane coincides with the source plane, $z = z' = 0$. The average relative numbers of the associated integration points for the evaluation of the tails of the Green's functions $G_{xx}^A(\rho; z, z')$ and $G_x^q(\rho; z, z')$ are shown in Table I. Based on the presented results, we can conclude that the DE formulas require less integration points and, as explained above, less CPU time to achieve the predefined accuracy.

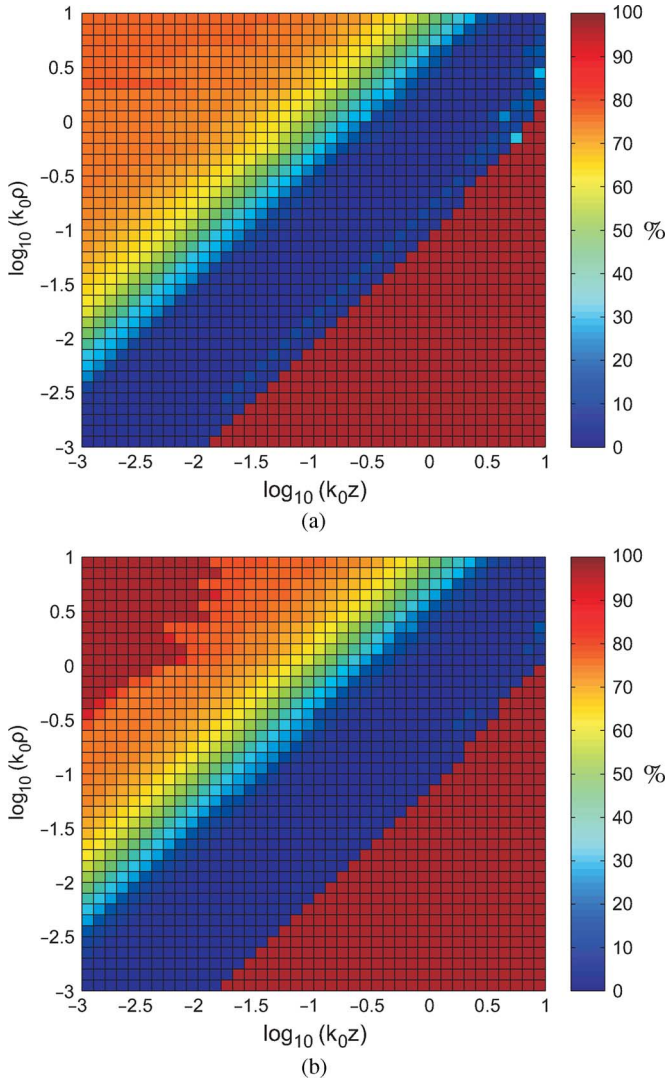

Fig. 5. Relative number of integration points $N_{\rm DE}/N_{\rm WA}$ (%) for a wide range of distances from the source. (a) Sommerfeld identity tail (18). (b) Derivative of the Sommerfeld identity tail (19).

TABLE I
AVERAGE RELATIVE NUMBER OF INTEGRATION POINTS NEEDED FOR THE EVALUATION OF SI TAILS

	N_{DE}/N_{WA} (%)
three-layer geometry	
$G_x^q\|_{f=8\ \rm GHz}$	77.25
$G_{xx}^A\|_{f=8\ \rm GHz}$	77.19
four-layer geometry	
$G_x^q\|_{f=1\ \rm GHz}$	77.37
$G_{xx}^A\|_{f=1\ \rm GHz}$	77.31
$G_x^q\|_{f=30\ \rm GHz}$	78.13
$G_{xx}^A\|_{f=30\ \rm GHz}$	78.38

V. CONCLUSION

In this manuscript, a novel technique for the fast and accurate computation of SI tails via direct integration, based on DE-type quadrature formulas is introduced. We have demonstrated the superior behavior of the proposed scheme, in terms of efficiency, over the traditional integration-then-summation procedure combined with the WA method, which is considered as the most proven method for the evaluation of the SI tails. More specifically, DE-type quadrature rules converge to the predefined accuracy, while reducing the overall computational cost roughly close to 25% compared to the WA method.

REFERENCES

[1] J. R. Mosig, "Arbitrary shaped microstrip structures and their analysis with a mixed potential integral equation," *IEEE Trans. Microw. Theory Tech.*, vol. 36, no. 2, pp. 314–323, 1988.
[2] K. A. Michalski, "The mixed-potential electric field integral equation for objects in layered media," *Arch. Elek. Ubertragung.*, vol. 39, no. 5, pp. 317–322, 1985.
[3] K. A. Michalski and D. Zheng, "Electromagnetic scattering and radiation by surfaces of arbitrary shape in layered media, Part 1: Theory," *IEEE Trans. Antennas Propag.*, vol. 38, no. 3, pp. 335–344, 1990.
[4] M. I. Aksun and G. Dural, "Clarification of issues on the closed-form Green's functions in stratified media," *IEEE Trans. Antennas Propag.*, vol. 53, no. 11, pp. 3644–3653, 2005.
[5] M. Yuan, T. K. Sarkar, and M. Salazar-Palma, "A direct discrete complex image method from the closed-form Green's functions in multilayered media," *IEEE Trans. Microw. Theory Tech.*, vol. 54, no. 3, pp. 1025–1032, 2006.
[6] V. N. Kourkoulos and A. C. Cangellaris, "Accurate approximation of Green's functions in planar stratified media in terms of a finite sum of spherical and cylindrical waves," *IEEE Trans. Antennas Propag.*, vol. 54, no. 5, pp. 1568–1576, May 2006.
[7] R. R. Boix, F. Mesa, and F. Medina, "Application of total least squares to the derivation of closed-form Green's functions for planar layered media," *IEEE Trans. Microw. Theory Tech.*, vol. 55, no. 2, pp. 268–280, 2007.
[8] A. G. Polimeridis, T. V. Yioultsis, and T. D. Tsiboukis, "A robust method for the computation of Green's functions in stratified media," *IEEE Trans. Antennas Propag.*, vol. 55, no. 7, pp. 1963–1969, 2007.
[9] N. Kinayman and M. I. Aksun, "Comparative study of acceleration techniques for integrals and series in electromagnetic problems," *Radio Sci.*, vol. 30, no. 6, pp. 1713–1722, 1995.
[10] K. A. Michalski, "Extrapolation methods for Sommerfeld integral tails," *IEEE Trans. Antennas Propag.*, vol. 46, no. 10, pp. 1405–1418, 1998.
[11] T. Hasegawa and A. Sidi, "An automatic integration procedure for infinite range integrals involving oscillatory kernels," *Numer. Algorithms*, vol. 13, no. 1, pp. 1–19, 1996.
[12] T. Ooura, "A continuous Euler transformation and its application to the Fourier transforms of a slowly decaying functions," *J. Comput. Appl. Math.*, vol. 130, no. 1–2, pp. 259–270, 2001.
[13] S. Singh and R. Singh, "Computation of Sommerfeld integrals using tanh transformation," *MOTL*, vol. 37, no. 3, pp. 177–180, 2003.
[14] T. Ooura, "A generalization of the continuous Euler transformation and its application to numerical quadrature," *J. Comput. Appl. Math.*, vol. 157, no. 2, pp. 251–259, 2003.
[15] M. Yuan and T. K. Sarkar, "Computation of the Sommerfeld integral tails using the matrix pencil method," *IEEE Trans. Antennas Propag.*, vol. 54, no. 4, pp. 1358–1362, 2006.
[16] H. Ogata and M. Sugihara, "Quadrature formulae for oscillatory infinite integrals involving the Bessel functions (in Japanese)," *Trans. Jpn. Soc. Industr. Appl. Math.*, vol. 8, no. 2, pp. 223–256, 1998.
[17] H. Takahasi and M. Mori, "Double exponential formulas for numerical integration," *Publ. RIMS, Kyoto Univ.*, vol. 9, no. 3, pp. 721–741, 1974.
[18] C. Frappier and P. Olivier, "A quadrature formula involving zeros of Bessel functions," *Math. Comp.*, vol. 60, no. 201, pp. 303–316, 1993.
[19] G. R. Grozev and Q. I. Rahman, "Quadrature formula with zeros of Bessel functions as nodes," *Math. Comp.*, vol. 64, no. 210, pp. 715–725, 1995.
[20] R. B. Ghanem, "Quadrature formulae using zeros of Bessel function as nodes," *Math. Comp.*, vol. 67, no. 221, pp. 323–336, 1998.
[21] K. A. Michalski, "Application of the complex image method to electromagnetic field computation in planar uniaxial multilayers," presented at the Workshop on Integral Techniques for Electromagnetics (INTELECT), Lausanne, Switzerland, 2007.
[22] J. R. Mosig and F. E. Gardiol, *A Dynamical Radiation Model for Microstrip Structures. Advances in Electronics and Electron Physics*. New York: Academic, 1982, pp. 139–237, (Eds).

[23] J. R. Mosig and F. E. Gardiol, "Analytical and numerical techniques in the Green's function treatment of microstrip antennas and scatterers," *IEE Proc., Part H—Microw., Opt. Antennas*, vol. 130, no. 2, pp. 175–182, 1983.
[24] J. R. Mosig, "Integral equation techniques," in *Numerical Techniques for Microwave and Milimeter-Wave Passive Structures*, T. Itoh, Ed. New York: Wiley, 1989, pp. 133–213.
[25] H. H. H. Homeier, "Scalar Levin-type sequence transformations," *J. Comput. Appl. Math.*, vol. 122, no. 1–2, pp. 81–147, 2000.
[26] T. Ooura and M. Mori, "A robust double exponential formula for Fourier-type integrals," *J. Comput. Appl. Math.*, vol. 112, no. 1–2, pp. 229–241, 1999.
[27] T. N. L. Patterson, "Algorithm 468: Algorithm for automatic numerical integration over a finite interval," *Commun. ACM*, vol. 16, no. 11, pp. 694–699, 1973.

Diversity On-Glass Antennas for Maximized Channel Capacity for FM Radio Reception in Vehicles

Seungbeom Ahn, Yong Soo Cho, and Hosung Choo

***Abstract*—This communication proposes a systematic design method to increase the diversity gain for vehicle on-glass antennas using the Pareto genetic algorithm. The initial antenna structure consists of two FM antennas printed on a rear window with horizontal conducting striplines. The position and the number of the vertical lines in the rear window were then determined using the Pareto genetic algorithm to maximize the channel capacity and average bore-sight gain of each antenna. The optimized antennas were built and mounted in a commercial sedan, and the antennas' performances, such as the reflection coefficient, radiation pattern, and channel capacity were measured. The measurements showed a matching bandwidth of around 15% and an average bore-sight gain of more than -12 dBi. The measured correlation coefficient of the two antennas was less than 0.6.**

***Index Terms*—Channel capacity, correlation coefficient, diversity on-glass antennas.**

I. Introduction

FM radio is one of the most popular communication systems utilized in current vehicle design [1]. Customers expect a high quality reception from their FM radios, although they drive their vehicles in various environments. Thus, most of the vehicle manufacturers put considerable effort into improving their radio systems and compete to offer their own performance standard in FM reception. An FM radio consists of a tuner, an amplifier, a connection cable, and a receiving antenna. Of these, the receiving antenna is probably the most important unit because of its critical effect on the reception performance.

Manuscript received February 12, 2010; revised June 10, 2010; accepted October 26, 2010. Date of publication December 03, 2010; date of current version February 02, 2011. This work was supported by the Hyundai Kia Motors and the IT R&D program of MKE/KEIT [KI002084, A Study on Mobile Communication System for Next-Generation Vehicle with Internal Antenna Array].

S. Ahn is with the RFID Team, Convergence R&D Center, LS Industrial Systems, Anyang 431-749, Korea (e-mail: sbahn@lsis.biz).
Y. S. Cho is with the School of Electronics and Electrical Engineering, Chung-Ang University, Seoul 156-756, Korea (e-mail: yscho@cau.ac.kr).
H. Choo is with the School of Electronic and Electrical Engineering, Hongik University, Seoul 121-791, Korea (e-mail: hschoo@hongik.ac.kr).

Color versions of one or more of the figures in this communication are available online at http://ieeexplore.ieee.org.
Digital Object Identifier 10.1109/TAP.2010.2096188

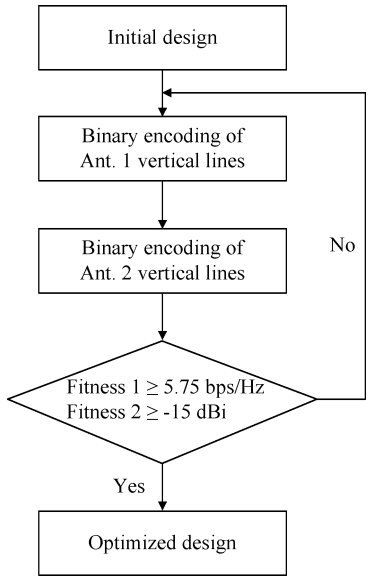

Fig. 1. Block diagram of the PGA design procedure.

Monopole type antennas, such as tuned-monopoles, micro-antennas, and shark fin antennas, have been widely used in numerous vehicle designs [2], [3]. These antennas, however, suffer from a lack of durability, high aerodynamic resistance, and an undesirable appearance, as they protrude from the vehicle's exterior. To mitigate these problems, on-glass antennas have been developed and are now commonly applied in modern vehicle designs. On-glass antennas also have the advantage of having a low manufacturing cost, due to the antennas being printed directly onto the vehicle window [4], [5]. However, they usually suffer from narrow matching bandwidth, low antenna gain, and radiation nulls, because the stripline of an on-glass antenna is printed onto the glass with a high dielectric loss. Also, the on-glass antennas show performance deterioration in urban environments where the channel characteristics are predominated by multi-path fading [6]. Recently, to improve the receiving performance, some luxury vehicles have employed diversity on-glass antennas systems that incorporate two separate antennas in a single window.

In this communication, we propose a systematic design method for diversity on-glass antennas that make them suitable for FM radio reception in a commercial sedan. The basic structure of the diversity on-glass antenna incorporates two FM antennas placed on the upper and lower areas of the rear window [7]–[9]. The horizontal lines of the antennas are commonly used as defroster lines, so the position and the number of the vertical lines were determined using the Pareto genetic algorithm (PGA) to maximize the channel capacity and average bore-sight gain of each antenna. The optimized on-glass antennas were built and mounted on a commercial sedan, and the antenna performance, such as the reflection coefficient and the bore-sight gain, were measured in a semi-anechoic chamber. The measurement showed a half-power bandwidth of around 15% and a bore-sight gain of over -20 dBi in the FM radio band. To confirm the diversity performance in a real situation, we measured the received FM signal power in an urban environment, where multi-path fading exists, which revealed low correlation coefficients of 0.52 between the diversity on-glass antennas.

II. Antenna Structure and Optimization

Fig. 1 shows a block diagram of the proposed design method for diversity on-glass antennas. The detailed designs of the antennas were